



Scattering of periodic surface waves by pile-group supported platform



Xiaoyu Guo^{a,b}, Benlong Wang^{a,b,*}, Chiang C. Mei^{a,c}, Hua Liu^{a,b}

^a Department of Engineering Mechanics, Shanghai Jiao Tong University, 200240, Shanghai, China

^b Ministry of Education Key Laboratory of Hydrodynamics, Shanghai Jiao Tong University, 200240, Shanghai, China

^c Department of Civil and Environmental Engineering, Massachusetts Institute of Technology, Cambridge, MA, USA

ARTICLE INFO

Keywords:

Scattering problem
Free surface wave
Homogenization
Eddy viscosity

ABSTRACT

A semi-analytical approach is proposed to solve the scattering of free surface waves around a platform supported by a pile array. Assuming periodic lattice configuration and strong contrast between cylinder spacing and typical wavelength, the multi-scale perturbation theory of homogenization is employed to derive the effective equations governing the macro-scale wave dynamics and the boundary-value problem of micro-scale flows within a unit cell. The constitutive coefficient in the macro-scale effective equations are computed from the solution of the micro-scale boundary-value problem, which is driven by the macro-scale pressure gradient. Flow separation is treated by the eddy viscosity model where the bulk eddy viscosity is determined by balancing the time-averaged rate of dissipation and the rate of work done by wave forces on the cylinders integrated over the entire platform region. The proposed semi-analytical approach is validated by comparisons with laboratory experiments for a pile-group supported platform in a wave flume. In addition field-scale wave scattering by a pile-group supported circular platform is investigated. For long waves, the maximum vertical force exerted on pile-group supported platform may reach 1.2 times of the value without piles. The maximum increase of the torque in transverse direction occurs for intermediate waves, which may reach 40% for the parameters discussed.

1. Introduction

Very large scale floating structures (VLFS) has been considered as a practically sustainable way for coastal and offshore development (Watanabe et al., 2004; Wang and Tay, 2011; Lamas-Pardo et al., 2015). The projects for residential or strategic purposes have been carried out, such as offshore airports, large storage facilities and wave energy converters (Singh and Babarit, 2014), pile group-supported offshore platforms and pier structures (Bonakdar and Oumeraci, 2015). There are basically two types of very large floating structures (VLFSs). One group is represented by Pontoon-type VLFS or MegaFloats, which stand on the sea level like a giant plate floating on water and are suitable for use in only calm waters. The other group is represented by the semi-submersible VLFS, which is raised by column tubes or small piles to minimize the effects of waves. In the present study, wave scattering around pile-group supported platform is investigated.

For pile group supported platform, group effects occur when the relative spacing, defined as the ratio of cylinder distance to diameter, are between 0.5 and 5.0 in practical applications (Bonakdar and Oumeraci, 2012). Hence, wave scattering around this kind of platform involves different scales, characterized by the pile diameter, pile spacing, wave

length and platform size. The flow field in the region with a large number of piles is complicated turbulence flow. The most direct method for this problem is to conduct 3D numerical simulation using RANS equations and associated turbulence model. However, the computational cost is too huge for current computer capability, and the unknown parameters for the turbulence closure model is also hard to be confirmed. In the past decades, wave scattering by finite dock has been solved mathematically in the frame of potential flow. Miles and Gilbert (1968), Mei and Black (1969), Garrett (1971) and Black et al. (1971) studied the scattering of surface waves by long or circular dock using eigenfunction expansion technique. Linton (2001) and Porter (2016) among others adopted Wiener-Hopf technique, residue calculus and the Green's function to solve the finite dock problem. These methods established solid foundations of the free surface wave scattering by an isolated floating body. In addition, wave scattering by multiple bodies have also been investigated based on potential flow theory. By using the multiple scattering technique, the whole phenomena of wave interactions with body arrays have been well solved (Spring and Monkmeyer, 1974; Simon, 1982; Linton and Evans, 1990). In terms of the diffraction characteristics of single member, a general diffraction problem involving a number of separated bodies has been solved exactly by Kagemoto and Yue (1986).

* Corresponding author. Department of Engineering Mechanics, Shanghai Jiao Tong University, 200240, Shanghai, China.

E-mail address: Benlongwang@sjtu.edu.cn (B. Wang).

Near-strapping phenomenon could be an important issue for free surface wave scattering around cylinder array. Recently, [Chen et al. \(2011\)](#) and [Chen and Lee \(2013\)](#) developed a fast semi-analytical method using the null-field integral equations to investigate free surface water wave scattering by an array of circular or elliptical shapes cylinders.

In the areas of large offshore platforms, wave-power extraction devices and offshore floating airports, [Kagemoto and Yue \(1993\)](#) proposed a general method that can solve the water-wave diffraction and radiation by a number of separate members in the context of linearized potential flow. As an extension of [Kagemoto and Yue \(1986\)](#), column-supported-type structures with up to 1280 and 5120 circular cylinders have been investigated by [Kashiwagi \(2000\)](#). Through this approach the wave patterns around the structures, deflection of the upper-deck and resonant phenomena can be investigated at reasonable computational costs.

As the number of piles dramatically increases, more realistic flow conditions need to be considered. For a platform supported by hundreds or thousands of small plies, the small structures may induce flow separation and vortex shedding, leading to wave energy dissipation due to viscous effects, especially for closely-spaced piles in group ([Bonakdar and Oumeraci, 2015](#)). The aforementioned approaches based on potential flow theory become unreliable. Due to the complexity of the flow field, experimental tests for different pile arrangement in [Bonakdar and Oumeraci \(2015\)](#) have contributed to the knowledge of the interaction between waves and pile group supported structures. Hydrodynamic forces on a pile within a group of piles in side by side arrangement and tandem arrangement have been studied by [Bonakdar and Oumeraci \(2012\)](#). However, the experimental investigation only focused on the local effect on a pile in a group with very few members. For VLFS, the number of piles supporting the platform can be of $\mathcal{O}(1000)$. Theories for the hydrodynamic forces imposed on the platform of VLFS are still wanting. Additionally, viscous dissipation of wave energy may significantly alter the wave intensity from one end to the other end of the very long platform. Hence, investigations of viscous effect on hydrodynamic loads of VLFSs are needed.

Besides the experimental studies, effective computational approach are needed to provide a fast and systematic prediction. Most existing techniques in three dimensional viscous computational fluid dynamics are not suitable for practical applications, when piles, platform and free surface are all present. If the piles are closely spaced, the commonly used Morison formulation, based on a single isolated pile, can not be applied. In recent years a new theory of wave propagation through piles groups has been advanced by the perturbation techniques of multiple scales, also known as homogenization, by [Mei et al. \(2011, 2014\)](#), [Guo et al. \(2014\)](#), [Wang et al. \(2015\)](#) and [Liu et al. \(2015\)](#). In this study, we extend their approach to investigate the wave scattering by a platform supported by a great number of piles. In the proposed method, the viscous flow model in the pile group region and non-viscous flow model outside are combined to solve the full problem. The approach is confirmed by experimental tests for wave scattering around a two-dimensional platform supported by arrays of a large number of piles. The theory is then extended to

field-scale wave scattering around a circular shape platform supported by piles.

2. Description of the problem

We study the scattering problem of water waves by a pile-group supported long platform partially immersed in a sea of finite constant depth h' . Two geometries are considered here: an infinitely long platform of width $2L'$ and a circular platform of radius R' , as sketched in [Fig. 1](#). Their drafts are denoted by D' . All piles are vertical, have the same diameter a' and form an array with the spacing $\mathcal{O}(\ell')$. Infinitesimal waves of characteristic frequency ω' and amplitude A' enter region beneath the platform from the open sea. The water depth is comparable with the wave length $2\pi/k'$, i.e., $k'h' = \mathcal{O}(1)$. The pile spacing is assumed to be much smaller than the typical wave length, or water depth, i.e., $k'\ell' \ll 1$.

The flow field can be divided into two parts: potential flow in the open water (away from the piles-supported platform) and viscous flow beneath the platform. In the following subsections, we give the model descriptions for these two regions respectively.

2.1. Potential flow in open water

In open water away from the platform, we ignore turbulence and viscosity. The dimensionless potential function ϕ satisfies the Laplace equation $\nabla^2\phi = 0$. Considering simple harmonic waves, linearity of the problem allows separation of the time factor as $(\phi, p) = (\Phi, P)e^{-it}$.

At first, let's consider a two-dimensional platform of finite length $2L$. For an incident wave in the form of $\zeta = \mathcal{A}e^{ik(X+L)-it}$, the potential in the exterior region can be expressed in terms of eigenfunctions as

$$\begin{aligned}\Phi_I &= -f_0 e^{-k_0(X+L)}, \quad \Phi_R = -\sum_{n=0}^{\infty} c_n f_n e^{k_n(X+L)}, \\ \Phi_T &= -\sum_{n=0}^{\infty} b_n f_n e^{-k_n(X-L)}\end{aligned}\quad (1)$$

with $k_0 = -ik$, k , k_n are real and positive, and satisfy $k_n \tan k_n h = -k \tanh kh$, $n = 1, 2, \dots$. In open water we have the following eigenfunctions, e.g. [Mei and Black \(1969\)](#); [Mei et al. \(2005\)](#).

$$f_0 = \frac{\sqrt{2} \cosh k(Z+h)}{(h + \sigma^{-1} \sinh^2 kh)^{1/2}}, \quad f_n = \frac{\sqrt{2} \cos k_n(Z+h)}{(h - \sigma^{-1} \sin^2 k_n h)^{1/2}} \quad (2)$$

where $\sigma = k \tanh kh$. The eigenfunctions are orthogonal in the region $-h \leq Z \leq 0$, i.e. $\int_{-h}^0 f_n f_m dZ = \delta_{nm}$ for $n, m = 0, 1, 2, \dots$. The incoming wave is from $X = -\infty$ towards the platform located between $X = \pm L$. c_0 and b_0 represent the reflection and transmission coefficients, respectively.

For simplicity, the amplitude of incident wave takes form of

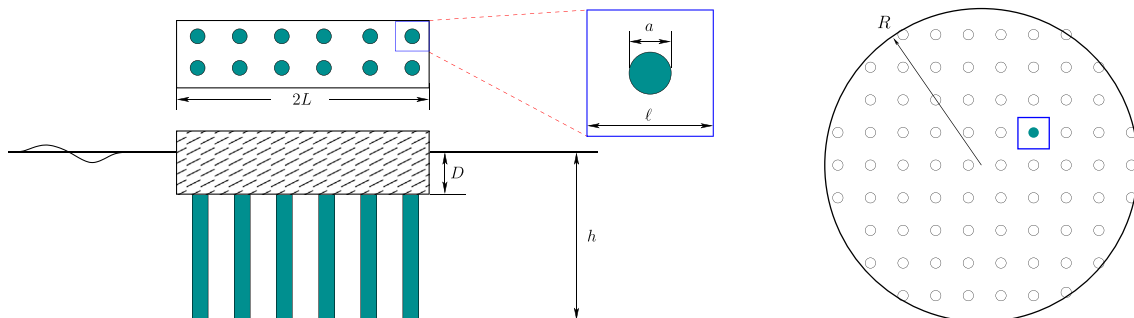


Fig. 1. Illustration of simplified platform supported by vertical piles. Left: a long platform of width $2L$, Right: a circular platform of radius R .

$$\mathcal{A} = -i \frac{\sqrt{2} \cosh kh}{(h + \sigma^{-1} \sinh^2 kh)^{1/2}} \quad (3)$$

For circular platform, we have the incident potential function:

$$\Phi_I = -f_0 e^{ikx} = \sum_{m=0}^{\infty} \phi_m^I \cos m\theta = -f_0 \sum_{m=0}^{\infty} i^m \varepsilon_m J_m(kr) \cos m\theta \quad (4)$$

where ε_m is Jacobi's symbol, $\varepsilon_0 = 1$ and $\varepsilon_m = 2$ for $m \geq 1$, e.g. Miles and Gilbert (1968). The general solution of Laplace equation in polar coordinates which satisfies the radiation condition at infinity is

$$\begin{aligned} \Phi_R &= \sum_{m=0}^{\infty} \phi_m^R(r, z) \cos m\theta \\ &= \sum_{m=0}^{\infty} \left[Q_{m0} \frac{H_m^{(1)}(kr)}{H_m^{(1)'}(kR)} f_0(z) + \sum_{n=1}^{\infty} Q_{mn} \frac{K_m(k_n r)}{K_m(k_n R)} f_n(z) \right] \cos m\theta \end{aligned} \quad (5)$$

2.2. Viscous flow beneath the platform

In Mei et al. (2014), wave propagation through a long pile group without the platform is studied by using the asymptotic technique of multiple scales. Their analysis has been applied to a marine forest of a circular area by Liu et al. (2015), and can be applied to the region beneath the platform, as sketched below. The incoming waves still dictate the scales of the dynamic pressure $[p] = \rho g A'$. The wavelength $1/k' = g/\omega'^2$ is the characteristic macro-length scale. Let us introduce the following dimensionless variables

$$\begin{aligned} x_i &= x'_i / \ell', \quad Z = k' z', \quad t = \omega' t', \quad h = k' h', \\ p &= p' / \rho g A', \quad (u_i, w) = (u'_i, w') / \omega' A', \quad \zeta = \zeta' / A' \end{aligned} \quad (6)$$

Where the horizontal coordinates are normalized by the microscale length ℓ' . For infinitesimal waves, the three dimensional flow between the piles are governed by the linearized Reynolds equations. The normalized continuity equation reads:

$$\frac{\partial u_i}{\partial x_i} + \varepsilon \frac{\partial w}{\partial Z} = 0 \quad (7)$$

Here we define $\varepsilon \equiv k' \ell' = \omega'^2 \ell' / g \ll 1$ which is a small ratio of micro-to-macro lengths, and dimensionless eddy viscosity $\sigma_e = \nu_e / \omega' \ell'^2 = \mathcal{O}(1)$. Assuming constant eddy viscosity to be determined later, the dimensionless horizontal and vertical momentum equations are

$$\varepsilon \frac{\partial u_i}{\partial t} = -\frac{\partial p}{\partial x_i} + \sigma_e \varepsilon \left(\frac{\partial^2 u_i}{\partial x_j \partial x_j} + \varepsilon^2 \frac{\partial^2 u_i}{\partial Z^2} \right) \quad (8)$$

$$\frac{\partial w}{\partial t} = -\frac{\partial p}{\partial Z} + \sigma_e \left(\frac{\partial^2 w}{\partial x_j \partial x_j} + \varepsilon^2 \frac{\partial^2 w}{\partial Z^2} \right) \quad (9)$$

Two-scale expansions are introduced, $x_i \rightarrow x_i + \varepsilon X_i$, $u_i \rightarrow u_i^{(0)} + \varepsilon u_i^{(1)}$, $w \rightarrow w^{(0)} + \varepsilon w^{(1)}$, $p \rightarrow p^{(0)} + \varepsilon p^{(1)}$. When high order terms at $\mathcal{O}(\varepsilon^2)$ are neglected, continuity Eq. (7) gives at $\mathcal{O}(1)$, $\mathcal{O}(\varepsilon)$

$$\frac{\partial u_i^{(0)}}{\partial x_i} = 0, \quad i = 1, 2 \quad (10)$$

$$\frac{\partial u_i^{(0)}}{\partial X_i} + \frac{\partial u_i^{(1)}}{\partial x_i} + \frac{\partial w^{(0)}}{\partial Z} = 0, \quad i = 1, 2 \quad (11)$$

At $\mathcal{O}(1)$, $\mathcal{O}(\varepsilon)$, the horizontal momentum Eq. (8) gives

$$-\frac{\partial p^{(0)}}{\partial x_i} = 0 \quad (12)$$

$$\frac{\partial u_i^{(0)}}{\partial t} = -\frac{\partial p^{(0)}}{\partial X_i} + \frac{\partial}{\partial x_j} \left(\tau_{ij}^{(1)} - p^{(1)} \delta_{ij} \right) \quad (13)$$

Here we define

$$\tau_{ij}^{(1)} = \sigma_e \left(\frac{\partial u_i^{(0)}}{\partial x_j} + \frac{\partial u_j^{(0)}}{\partial x_i} \right) \quad (14)$$

for later use. Eq. (12) implies that pressure $p^{(0)}$ varies only at macro length scale X_i .

With two scale expansions, the vertical momentum Eq. (9) becomes at the leading order

$$\frac{\partial w^{(0)}}{\partial t} = -\frac{\partial p^{(0)}}{\partial Z} + \sigma_e \frac{\partial^2 w^{(0)}}{\partial x_j \partial x_j} \quad (15)$$

On the surface of the vertical cylinders

$$u_i = w = 0, \quad \vec{x}, Z \in S_B \quad (16)$$

Different from Mei et al. (2014), we add the kinematic boundary condition on the platform bottom in addition to the condition at the seabed, i.e.

$$u_i = w = 0, \quad Z = -D, \quad |X| < L \quad \text{or} \quad \sqrt{X^2 + Y^2} < R \quad (17)$$

2.2.1. Cell problem on the microscale

Considering simple harmonic waves and assuming $f(x_i, Z, t) = \text{Re}[\tilde{f}(x_i, Z) e^{-it}]$, we only need to study the complex amplitude $\tilde{f}(x_i, Z)$.

From the leading order horizontal momentum Eq. (12), we find the leading order pressure $p^{(0)} = p^{(0)}(X_i, Z, t)$ to be independent of micro-scale coordinate x_i . In view of linearity of Eqs. (8)–(9), we assume the following solutions for the micro-scale flow in the cell

$$\tilde{u}_i^{(0)} = -K_{ij}(\vec{x}) \frac{\partial \tilde{p}^{(0)}}{\partial x_j}, \quad \tilde{p}^{(1)} = -A_j(\vec{x}) \frac{\partial \tilde{p}^{(0)}}{\partial x_j}, \quad \tilde{w}^{(0)} = -W(\vec{x}) \frac{\partial \tilde{p}^{(0)}}{\partial Z} \quad (18)$$

Substituting these assumptions into the continuity Eq. (7) and momentum Eq. (8), we have

$$\frac{\partial K_{ij}}{\partial x_j} = 0, \quad -iK_{ij} = \delta_{ij} + \sigma_e \frac{\partial^2 K_{ij}}{\partial x_k \partial x_k} - \frac{\partial A_j}{\partial x_i}, \quad x_i \in \Omega_f \quad (19)$$

Eq. (19) must be solved in the fluid part Ω_f in the unit cell of area Ω , subjected to the boundary conditions on the cylinders $K_{ij} = 0$, $x_i \in S_B$ and periodicity boundaries $K_{ij}, A_j: \Omega \rightarrow \text{periodic}$. For uniqueness, $\langle A_j \rangle = 0$ is required. We define the cell-averaged variable $\langle f \rangle$ as $\langle f \rangle = \iint_{\Omega_f} f dx dy / \Omega$. After solving the canonical cell problem by Finite Element Method (FEM), we obtain the complex permeability $\mathcal{K}_{ij} = \langle K_{ij} \rangle$ and get Darcy's law

$$\langle \tilde{u}_i^{(0)} \rangle = -\mathcal{K}_{ij} \partial \tilde{p}^{(0)} / \partial x_j \quad (20)$$

The vertical momentum equation, i.e. the leading order of (9) becomes

$$-iW = 1 + \sigma_e \frac{\partial^2 W}{\partial x_j \partial x_j}, \quad x \in \Omega_f, -h < z < -D \quad (21)$$

with boundary conditions

$$W = 0, \quad (x_i, Z) \in S_B \quad \text{and} \quad Z = -D, -h \quad (22)$$

and

$$W : \Omega - \text{periodic} \quad (23)$$

The cell boundary value problem can be solved by FEM. The boundary layers over seabed and beneath the bottom of platform are neglected in the present work, therefore Eq. (21) is solved in horizontal two dimensional space, i.e. $W = W(x_i)$, $i = 1, 2$, and is independent of the macro-coordinate Z . We define the cell-averaged W as $\mathcal{W} = \langle W \rangle$ for the permeability of the vertical component.

In the cell problem, dimensionless viscosity $\sigma_e = \nu_e / \omega \ell^2$ is unknown, which is determined by the iterative method in section 2.3. During the iteration, the horizontal and vertical cell problems are solved numerically based on the known eddy viscosity obtained from the previous iteration. The numerical computation by the finite element method are similar to those in Guo et al. (2014).

For this cell boundary-value problem, we can show that: $K_{11}(x, y) = K_{22}(y, x)$ and both are even in x and y , $K_{12} = K_{21}$ and they are symmetric with respect to the diagonals $x - y = 0$ and $x + y = 0$. For the symmetric cell geometry, the cell problem is isotropic, and the complex permeability can be expressed as $\mathcal{K}_{ij} = \mathcal{K} \delta_{ij}$. Sample results for the cell problem are shown in Fig. A.12.

2.2.2. Macro-scale problem

Let us denote the cell averaged velocities at the leading order as

$$\langle \tilde{u}_i^{(0)} \rangle, \langle \tilde{w}^{(0)} \rangle = \frac{1}{\Omega} \iint_{\Omega_f} \left(u_i^{(0)}, w^{(0)} \right) dx dy \quad (24)$$

$\langle \tilde{u}_i^{(0)} \rangle$ and $\langle \tilde{w}^{(0)} \rangle$ are macro-scale velocities depending on the macro-scale coordinates X_i and Z . Cell averaging of continuity Eq. (11) gives

$$\Omega \left(\frac{\partial \langle \tilde{u}_i^{(0)} \rangle}{\partial X_i} + \frac{\partial \langle \tilde{w}^{(0)} \rangle}{\partial Z} \right) + \iint_{\Omega_f} \frac{\partial u_i^{(1)}}{\partial x_i} dx dy = 0 \quad (25)$$

Using Gauss theorem, periodicity and no-slip boundary conditions, the integral above is zero. Hence we obtain the cell averaged continuity equation

$$\frac{\partial \langle \tilde{u}_i^{(0)} \rangle}{\partial X_i} + \frac{\partial \langle \tilde{w}^{(0)} \rangle}{\partial Z} = 0 \quad (26)$$

The cell averages of the horizontal and vertical momentum Eqs. (13) and (15) are

$$-i \langle \tilde{u}_i^{(0)} \rangle = -\mathcal{N} \frac{\partial \tilde{p}^{(0)}}{\partial X_i} - \alpha_{ik} \frac{\partial \tilde{p}^{(0)}}{\partial X_k} \quad (27)$$

$$-i \langle \tilde{w}^{(0)} \rangle = -\mathcal{N} \frac{\partial \tilde{p}^{(0)}}{\partial Z} - \beta \frac{\partial \tilde{p}^{(0)}}{\partial Z} \quad (28)$$

where

$$\alpha_{ik} = \frac{1}{\Omega} \oint ds \left[\sigma_e \left(\frac{\partial K_{ik}}{\partial x_j} + \frac{\partial K_{jk}}{\partial x_i} \right) - A_k \delta_{ij} \right] n_j, \quad (29)$$

$$\beta = \frac{\sigma_e}{\Omega} \oint ds \frac{\partial W}{\partial x_j} n_j \quad (30)$$

do not depend on the vertical coordinate Z . Herein, \mathcal{N} is the porosity which is defined as Ω_f / Ω .

Substituting the momentum Eqs. (27) and (28) into the continuity Eq. (26), we have the general inhomogeneous and anisotropic Laplace-like equation for the pressure:

$$\frac{\partial}{\partial X_i} \left(\mathcal{K} \frac{\partial \tilde{p}^{(0)}}{\partial X_i} \right) + \mathcal{W} \frac{\partial^2 \tilde{p}^{(0)}}{\partial Z^2} = 0 \quad (31)$$

using the relationships of $\alpha_{11} = \alpha_{22} = -\mathcal{N} - i\mathcal{K}$, $\alpha_{12} = \alpha_{21} = 0$ and $\beta = -\mathcal{N} - i\mathcal{W}$ (See Appendix A).

In their study of waves through an aquatic forest, Liu et al. (2015) obtained the same governing equation as (31). Because the eddy viscosity ν_e is assumed to be constant on the macro-scale, both \mathcal{K} and \mathcal{W} are constants. This simplification gives predictions that are verified by their experiments. In the present study, the same assumption is adopted. Consequently, (31) becomes a homogeneous and anisotropic Laplace equation:

$$\mathcal{K} \frac{\partial^2 \tilde{p}^{(0)}}{\partial X_i \partial X_i} + \mathcal{W} \frac{\partial^2 \tilde{p}^{(0)}}{\partial Z^2} = 0 \quad (32)$$

The cell averaged macro-scale flow is bounded by the platform bottom $Z = -D$ and seabed $Z = -h$. At these two boundaries, the no-penetration conditions reduce to

$$\frac{\partial \tilde{p}^{(0)}}{\partial Z} = 0, \quad Z = -D, -h \quad (33)$$

for $|X| < L$ two dimensional finite platform, or $r < R$ circular platform.

At the interface of piles group and open water with outer normal vector \mathbf{n}_0 , we have

$$\frac{\partial \tilde{\Phi}}{\partial X} = \langle \tilde{u} \rangle n_0, \quad -h < Z < -D \quad (34)$$

$$i\tilde{\Phi} = \tilde{p}^{(0)} \quad -h < Z < -D \quad (35)$$

at $X = \pm L$ of finite platform, or $r = R$ for circular platform respectively.

The solution of this macro-scale problem can be found easily and coupled with the potential theory away from the platform and piles.

2.3. Determination of the eddy viscosity

We must now determine the value of the constant bulk eddy viscosity ν_e . This is accomplished by using the concept of energy balance as that in Guo et al. (2014); Wang et al. (2015); Liu et al. (2015). The time-averaged energy dissipation rate in the cylinder array is equivalent to the time-averaged rate of work done by the drag force.

$$\frac{1}{2} \rho C_{D,rms} a' \iint_S dS \int_{-h}^{-D'} dz' \overline{\langle u_i^{(0)} \rangle^2} \left| \langle u_i^{(0)} \rangle \right| = 2\rho \nu_e \iiint_V \overline{e'_{ij} e'_{ij}} dV \quad (36)$$

in which $e'_{ij} = (\partial u_i^{(0)} / \partial x_j + \partial u_j^{(0)} / \partial x_i) / 2$, and overline denotes the time averages over a wave period. In (36), only the strain rates of leading order have been included. To be evaluated at the end of this subsection, $C_{D,rms}$ is the root mean square force coefficient during an oscillation cycle as that defined by Maull and Milliner (1978).

The dimensionless permeability is $\mathcal{K} = \rho \omega' \mathcal{K}'$. For the circular platform, we have $\partial / \partial X \rightarrow \partial / \partial r$ and $\partial / \partial Y \rightarrow \partial / \partial \theta$. Using (18), we can find the expression of the constant bulk ν_e in terms of pressure gradient as

$$\nu_e = \frac{\frac{2}{3\pi} C_{D,rms} a' \omega' A' |\mathcal{K}'|^3 \iint_S dS \int_{-h}^{-D} \left(\left| \frac{\partial \tilde{p}^{(0)}}{\partial r} \right|^2 + \left| \frac{\partial \tilde{p}^{(0)}}{r \partial \theta} \right|^2 \right)^{3/2} dZ}{\iint_S dS \left[\mathcal{F}_{\mathcal{K}} \int_{-h}^{-D} \left| \frac{\partial \tilde{p}^{(0)}}{\partial r} \right|^2 dZ + \mathcal{F}_{\mathcal{W}} \int_{-h}^{-D} \left| \frac{\partial \tilde{p}^{(0)}}{r \partial \theta} \right|^2 dZ + \mathcal{F}_{\mathcal{W}} \int_{-h}^{-D} \left| \frac{\partial \tilde{p}^{(0)}}{\partial Z} \right|^2 dZ \right]} \quad (37)$$

in which \mathcal{K} is constant, $\mathcal{F}_{\mathcal{K}}$, $\mathcal{F}_{\mathcal{W}}$, and $\mathcal{F}_{\mathcal{W}}$ are calculated from the cell problem, S is the area of the platform region.

$$\mathcal{F}_{\mathcal{K}} = \iint_{\Omega_j} dx dy \left[\left| \frac{\partial K_{21}}{\partial y} \right|^2 + \frac{1}{2} \left(\left| \frac{\partial K_{11}}{\partial y} \right|^2 + \left| \frac{\partial K_{21}}{\partial x} \right|^2 \right) + \Re \left(\frac{\partial K_{11}^*}{\partial y} \frac{\partial K_{21}}{\partial x} \right) \right] \quad (38)$$

$$\mathcal{F}_{\mathcal{W}} = \iint_{\Omega_j} dx dy \left[\left| \frac{\partial K_{22}}{\partial y} \right|^2 + \frac{1}{2} \left(\left| \frac{\partial K_{12}}{\partial y} \right|^2 + \left| \frac{\partial K_{22}}{\partial x} \right|^2 \right) + \Re \left(\frac{\partial K_{12}^*}{\partial y} \frac{\partial K_{22}}{\partial x} \right) \right] \quad (39)$$

$$\mathcal{F}_{\mathcal{W}} = \iint_{\Omega_j} \frac{1}{2} \left(\left| \frac{\partial W}{\partial x} \right|^2 + \left| \frac{\partial W}{\partial y} \right|^2 \right) dx dy \quad (40)$$

Herein, K_{11}^* and K_{12}^* denote the complex conjugate of K_{11} and K_{12} .

For 2D problem of an infinitely long platform, ν_e can be calculated from (37) by setting $\partial/\partial r = \partial/\partial X$ and $\partial\tilde{p}^{(0)}/\partial\theta = 0$.

We now turn to the drag coefficient $C_{D,rms}$. In present work, the presence of the platform eliminates the effect of free surface wave. Therefore, the drag coefficient can be taken from experiments in the absence of surface waves, unlike that used in Liu et al. (2015) where the upper boundary of the marine forest is free surface.

For steady flows through emergent and submerged cylinder arrays in open channels, Cheng and Nguyen (2011) proposed the following formula based on extensive experimental records:

$$C_{D\infty} = \frac{50}{Re_v^{0.43}} + 0.7 \left[1 - \exp \left(- \frac{Re_v}{15,000} \right) \right] \quad (41)$$

Here $Re_v = \langle U' \rangle r_v' / \nu$ is the Reynolds number based on the hydraulic radius $r_v' = \frac{\pi}{4} a' (1 - \phi) / \phi$ with ϕ being the solid fraction. $\langle U' \rangle$ is the mean velocity in the cylinder array region. Reynolds number Re_v ranges from 7.3×10^3 to 2.5×10^5 . Since $\tilde{u}_i^{(0)}$ depends on ν_e , (37) is an implicit equation for the eddy viscosity ν_e .

Bearman et al. (1979) presented measurements of a series of two-dimensional bodies in plane oscillatory flow for $K_C = \langle U' \rangle T' / a'$ values between 3 and 70, where $\langle U' \rangle$ is the ambient velocity amplitude, T' the wave period and a' the cylinder diameter. Their finding that the drag force increases due to returning eddies has been explained by Falin (1998). Using the original experimental data by Bearman et al. (1979), an empirical formulation can be obtained as

$$\frac{C_{D,rms}}{C_{D\infty}} = 8.745 K_C^{-1.155} + 1, \quad 3 \leq K_C \leq 70 \quad (42)$$

for circular cylinder. Our $C_{D,rms}$ is calculated from (42) by using $C_{D\infty}$ from (41).

3. Macroscale solution and experiments for 2D platform

3.1. Macroscale solution

For simple harmonic waves, linearity of the problem allows separation of the time factor as follows: $(\Phi, P) = (\tilde{\Phi}, \tilde{p}^{(0)}) e^{-it}$. For a long platform of finite width, numerical solution of Eq. (32) is needed, where \mathcal{K} and \mathcal{W} are constants. In terms of the pressure gradient, the matching conditions for continuity of velocity (34) read:

$$\frac{\partial \tilde{\Phi}^{(0)}}{\partial X} = \begin{cases} -\mathcal{K} \frac{\partial \tilde{p}^{(0)}}{\partial X} & -h \leq Z < -D \\ 0 & -D \leq Z < 0 \end{cases} \quad (43)$$

at $X = \pm L$.

In view of the boundary conditions (33), the general solution of $\tilde{p}^{(0)}$ can be expressed in terms of eigenfunctions F_n as

$$\tilde{p}^{(0)}(X, Z) = \sum_{n=0}^{\infty} P_n(X) F_n(Z) \quad (44)$$

Since \mathcal{K} and \mathcal{W} are constant, the eigenfunctions are $F_0 = 1/\sqrt{h-D}$, $F_n = \sqrt{2} \cos K_n(Z+h)/\sqrt{h-D}$, $n = 1, 2, \dots$ with $\lambda_n = K_n \sqrt{\mathcal{W}/\mathcal{K}}$ and $K_n = n\pi/(h-D)$, the eigenfunctions are orthogonal for $-h \leq Z < -D$, i.e. $\int_{-h}^{-D} F_n F_m dZ = \delta_{nm}$ for $n, m = 0, 1, 2, \dots$

Values of \mathcal{K} and \mathcal{W} are plotted in Fig. 2 for typical cylinder arrays and a fixed eddy viscosity $\nu_e = 1.0E-3$ m²/s. From (20), we have the magnitude of \mathcal{K} and \mathcal{W} measuring the ratio between the velocity and a given pressure gradient. The imaginary part relates to the phase lag between velocity and pressure gradient. For very long waves, the phase lag approaches to zero, indicating that the velocity is in phase with the pressure gradient. Computing the cell problems with different porosity, numerical results in Fig. 3 show that the imaginary part of \mathcal{K} and \mathcal{W} decreases linearly with the size of cylinder a/ℓ . When the pressure gradient is fixed, the velocity magnitude decrease when a/ℓ increases. As a limiting case $\mathcal{N} = 1$ when the radius of cylinder decreases to 0, we have $\mathcal{K} = \mathcal{W} = i$.

The potential in the exterior region are taken in form of (1). For finite platform in 2D space, general solution of Eq. (32) is rewritten as

$$P_0(X) = p_0 X + q_0, \quad P_n(X) = p_n \sinh \lambda_n X + q_n \cosh \lambda_n X, \quad n = 1, 2, \dots \quad (45)$$

with $\lambda_n = K_n \sqrt{\mathcal{W}/\mathcal{K}}$, p_n and q_n are complex coefficients to be determined from the other boundary conditions. We keep the constant

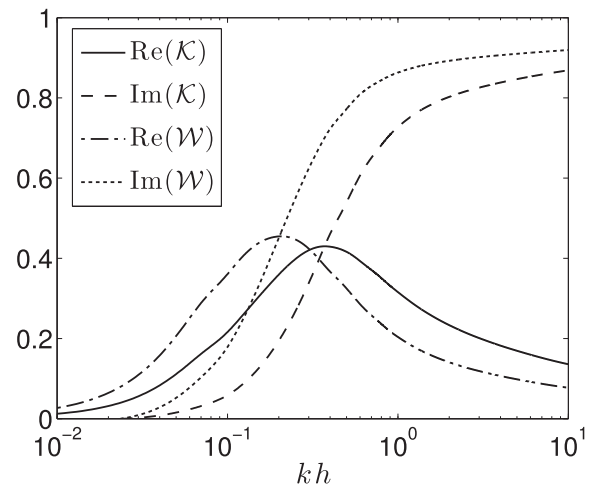


Fig. 2. Comparison of \mathcal{K} and \mathcal{W} versus kh . Parameters: $a'/\ell' = 0.1$, $\mathcal{N} = 0.9686$, $\nu_e = 1.0E-3$ m²/s, $h' = 0.5$ m, $\ell' = 0.08$ m.

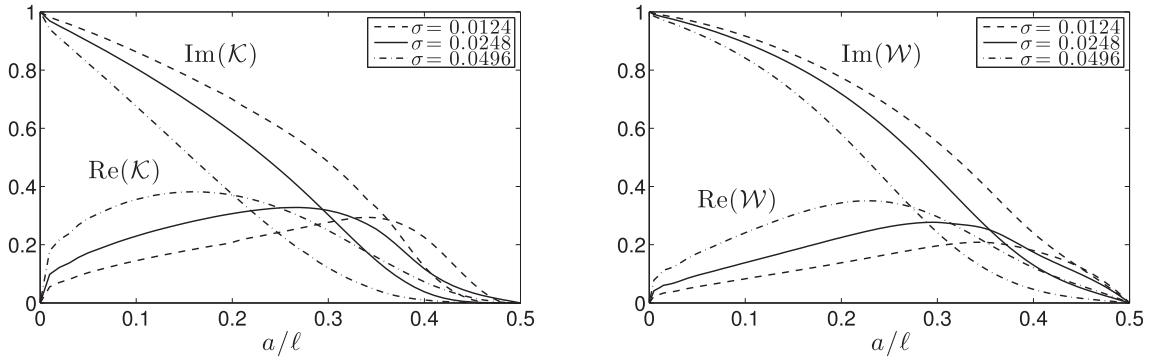


Fig. 3. Comparison of \mathcal{K} and \mathcal{W} for different cylinder diameter a'/ℓ' . Parameters: $h' = 0.5\text{m}$, $\ell' = 0.08\text{m}$.

pressure q_0 to study the pressure force exerted on platform. In fact, we found it is vital to include q_0 , as discussed in early work (Garrett, 1971).

3.1.1. Matching conditions at $x = -L$

Continuity of pressure (35) at $X = -L$ requires

$$f_0(1 + c_0) + \sum_{n=1}^N c_n f_n = i \left[(q_0 - p_0 L) F_0 + \sum_{n=1}^N (-p'_n + q'_n) F_n \right] \quad (46)$$

where $p'_n = p_n \sinh \lambda_n L$ and $q'_n = q_n \cosh \lambda_n L$ for $n = 1, \dots, N$.

On the open water side $X = -L$, the velocity can be expressed in terms of potential functions (1) as $\mathcal{W}^-(Z) = \partial(\Phi_I + \Phi_R)/\partial X$. Integrating $\mathcal{W}^-(Z)$ with f_n from $Z \in (-h, 0)$, we get

$$\langle \mathcal{W}^-, f_n \rangle = \int_{-h}^0 \mathcal{W}^- f_n dZ = \begin{cases} k_0(1 - c_0) & n = 0 \\ -k_n c_n & n \geq 1 \end{cases} \quad (47)$$

Under platform, according to the definition we have $\mathcal{W}^-(Z) = -\mathcal{K} \partial P / \partial X$. Integrating $\mathcal{W}^-(Z)$ with F_n for $Z \in (-h, -D)$, we have

$$\langle \mathcal{W}^-, F_n \rangle = -\mathcal{K} \begin{cases} p_0 & n = 0 \\ \lambda_n \left(\frac{p'_n}{\mathcal{T}_n} - q'_n \mathcal{T}_n \right) & n \geq 1 \end{cases} \quad (48)$$

in which $\mathcal{T}_n = \tanh \lambda_n L$. Substituting (47) (48) into (46), we get

$$f_0 \left(2 - \frac{\langle \mathcal{W}^-, f_0 \rangle}{k_0} \right) = \sum_{n=1}^N \frac{\langle \mathcal{W}^-, f_n \rangle f_n}{k_n} + i \frac{L}{\mathcal{K}} \langle \mathcal{W}^-, F_0 \rangle F_0 + i q_0 F_0 + i \sum_{n=1}^N (-p'_n + q'_n) F_n \quad (49)$$

3.1.2. Matching conditions at $x = L$

From the condition $i\Phi = P$ we have

$$b_0 f_0 + \sum_{n=1}^N b_n f_n = i \left[(p_0 L + q_0) F_0 + \sum_{n=1}^N (p'_n + q'_n) F_n \right] \quad (50)$$

At $X = L$, the velocity \mathcal{W}^+ can be expressed in terms of potential function as $\mathcal{W}^+ = \partial \Phi_T / \partial X$. Integrating \mathcal{W}^+ with f_n from $Z \in (-h, 0)$, we get

$$\langle \mathcal{W}^+, f_n \rangle = k_n b_n, \quad n = 0, 1, 2, \dots \quad (51)$$

Under the platform, $\mathcal{W}^+ = -\mathcal{K} \partial P / \partial X$, recalling the definition of p'_n and q'_n and integrating \mathcal{W}^+ with F_n for $Z \in (-h, -D)$, we get

$$\langle \mathcal{W}^+, F_n \rangle = -\mathcal{K} \begin{cases} p_0 & n = 0 \\ \lambda_n \left(\frac{p'_n}{\mathcal{T}_n} + q'_n \mathcal{T}_n \right) & n \geq 1 \end{cases} \quad (52)$$

Substituting (51) (52) into (50), we get

$$-f_0 \frac{\langle \mathcal{W}^+, f_0 \rangle}{k_0} = \sum_{n=1}^N \frac{\langle \mathcal{W}^+, f_n \rangle f_n}{k_n} + i \frac{L}{\mathcal{K}} \langle \mathcal{W}^+, F_0 \rangle F_0 - i q_0 F_0 + i \sum_{n=1}^N (p'_n q'_n) F_n \quad (53)$$

With (48) and (52), we get the values of p'_n and q'_n :

$$p'_n = -\mathcal{T}_n \langle \mathcal{W}^- + \mathcal{W}^+, F_n \rangle / (2\lambda_n \mathcal{K}), \quad q'_n = \langle \mathcal{W}^- - \mathcal{W}^+, F_n \rangle / (2\lambda_n \mathcal{K} \mathcal{T}_n) \quad (54)$$

Integrating (53) and (49) with F_0 for $Z \in (-h, -D)$, we get

$$i q_0 = G_{00} + \sum_{n=0}^N G_{n0} \langle \mathcal{W}^+ - \mathcal{W}^-, f_0 \rangle / (2k_n) \quad (55)$$

in which $G_{00} = \langle f_0, F_0 \rangle$ and $G_{n0} = \langle f_n, F_0 \rangle$ for arbitrary n .

3.1.3. Solution procedure

The final governing Eqs. (49) and (53) can be solved by using Ritz method (Mei and Black, 1969). Defining $\mathcal{W}^- = \sum_{m=0}^M A_m F_m(Z)$ and $\mathcal{W}^+ = \sum_{m=0}^M B_m F_m(Z)$, there are $2(M+1)$ unknowns A_m and B_m . Finally, at each point Z_s in $Z \in (-h, -D)$, we have following two equations according to (49) and (53):

$$\begin{aligned} f_0(Z_s) \left(2 - \frac{1}{k_0} \sum_{m=0}^M A_m G_{0m} \right) &= \sum_{m=0}^M A_m \left(\sum_{n=1}^N G_{nm} \frac{f_n(Z_s)}{k_n} \right) \\ &+ \frac{iL}{\mathcal{K}} A_0 F_0(Z_s) + \left[G_{00} + \sum_{n=0}^N \sum_{m=0}^M \frac{(B_m - A_m) G_{n0} G_{0m}}{2k_n} \right] F_0(Z_s) \\ &+ \frac{i}{2\mathcal{K}} \sum_{m=1}^M \left[\left(\mathcal{T}_m + \frac{1}{\mathcal{T}_m} \right) A_m + \left(\mathcal{T}_m - \frac{1}{\mathcal{T}_m} \right) B_m \right] \frac{F_m(Z_s)}{\lambda_m} \end{aligned} \quad (56)$$

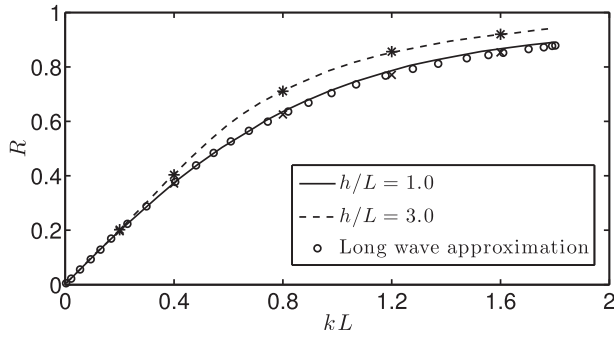


Fig. 4. Reflection coefficient for a finite platform with zero draught $D = 0$. Cross mark and Asterisk mark represent present results for $h/L = 1.0$ and $h/L = 3.0$. The lines are theoretical results of Mei and Black (1969).

$$\begin{aligned}
 & -\frac{f_0(Z_s)}{k_0} \sum_{m=0}^M B_m G_{0m} = \sum_{m=0}^M B_m \left(\sum_{n=1}^N G_{nm} \frac{f_n(Z_s)}{k_n} \right) + \frac{iL}{\mathcal{H}} B_0 F_0(Z_s) \\
 & - \left[G_{00} + \sum_{n=0}^N \sum_{m=0}^M \frac{(B_m - A_m) G_{n0} G_{0m}}{2k_n} \right] \\
 & + \frac{i}{2\mathcal{H}} \sum_{m=1}^M \left[\left(\mathcal{F}_m - \frac{1}{\mathcal{F}_m} \right) A_m + \left(\mathcal{F}_m + \frac{1}{\mathcal{F}_m} \right) B_m \right] \frac{F_m(Z_s)}{\lambda_m}
 \end{aligned} \quad (57)$$

for $s = 0, 1, 2, \dots, M$. Herein $G_{0m} = \langle f_0, F_m \rangle$ for $m = 0, 1, 2, \dots$, and $G_{nm} = \langle f_n, F_m \rangle$ for $n, m = 0, 1, 2, \dots$. The linear matrix can be solved easily with Mathematica. After obtaining the value of A_m and B_m , we can calculate c_0 and b_0 from (47) and (51) as $c_0 = 1 - \sum_{m=0}^M A_m G_{0m}/k_0$ and $b_0 = \sum_{m=0}^M B_m G_{0m}/k_0$. The constant pressure q_0 under the platform can be calculated from (55) once A_m and B_m are known. The other coefficients c_n, b_n, p_n, q_n can be calculated by the definition (47) (51) (54). Therefore all the potential and pressure field are obtained. Note that the reflection coefficient is given by $R = c_0 e^{2ikL}$, the transmission reflection is $T = b_0 e^{2ikL}$.

There are two parameters M and N in the truncated eigenfunction expansions. For both long wave and short wave, $M \sim N = 100$ ensures the results have a relative error less than $1.0E-4$.

3.2. Numerical validation

Preliminary verifications of the calculation procedure are examined for open water flows (platform without piles) by setting $\mathcal{H} = \mathcal{W} = i$ and the porosity $\mathcal{N} = 1$. To verify present numerical solution, we compare the numerical results with Stoker's solution for a thin plate slab with $D = 0$. The analytical reflection coefficient is $R = ikhe^{2ikh}/(1 + ikh)$ under long wave approximation (Stoker, 1958). The half length of the platform is $L = h$. It was found by Mei and Black (1969) that the Stoker's solution was surprisingly good for all practically values of kh when $L = h$. Fig. 4 shows

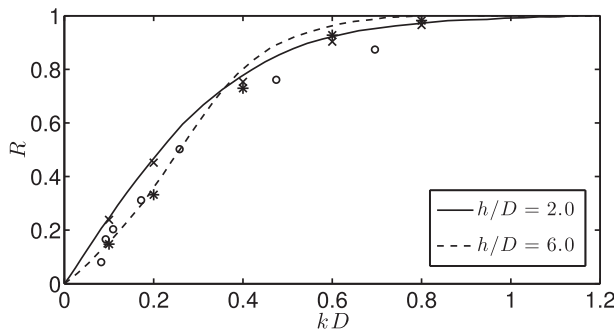


Fig. 5. Reflection coefficient for open water flow with $L/D = 1$. Cross mark and Asterisk mark represent present results for $h/D = 2.0$ and $h/D = 6.0$. The lines are theoretical results cited from Mei and Black (1969), circle is Kincaid's experiment for $h/D = 6.17$.

reflection coefficient for a finite platform with zero draft $D = 0$. The present numerical solution agrees well with Stoker's long wave approximation, which shows the same tendency as Mei and Black (1969). Another verification of the calculation procedure is examined through comparison of the reflection coefficients for open water flow with $L/D = 1$ as shown in Fig. 5. These two verifications demonstrate the present code works for open water problems. By using proper values of \mathcal{H} and \mathcal{W} in the code, we can calculate the full problem straightforwardly.

3.3. Experiments and verification for 2D finite length platform supported by cylinder arrays

An experiment have been conducted in a wave flume of width 0.8 m and length 55 m at Shanghai Jiao Tong University, China. Waves were generated at the upstream end of the flume by a piston-type wave maker. At the other end of the flume, a wave-absorbing beach with 1:6 slope composted with porous media was built to minimize wave reflection. The pile-group supported platform was placed at 16 m away from the wave maker. Six capacitance wave gauges were installed at each side of the platform. Four gauges were used to measure the reflected waves and two for transmission waves, at two different locations respectively. Reflection coefficient is obtained involving two fixed wave gauges using the classical method as described by Goda and Suzuki (1976). The incoming wave parameters are listed in Table 1.

The model pile was made from aluminum and had diameter $d' = 3$ cm and height $H'_c = 30$ cm. To fix the cylinders, a rectangular panel with 0.8 m wide was made and fixed at the bottom of the flume. The cylinders were uniformly spaced at $\ell' = 8$ cm apart with the porosity $\mathcal{N} = 0.89$, i.e., the cell size is 8 cm. The model of the piles-supported platform with length $2L' = 100$ cm and draft $D' = 10$ cm was installed in the flume of water depth $h' = 40$ cm as shown in Fig. 6. There are 10×12 cylinders installed beneath the platform. Fourteen tests with different wave periods and equal wave amplitude $A' = 2$ cm were performed as listed in Table 1. In the experiment, each case is repeated three times on the average to ensure the repeatability and accuracy. When the length scale is 1:50 in nearshore region, the water depth, cylinder diameter and cylinder space in the field scale are 20 m, 1.5 m and 4 m corresponding to present experimental parameters.

Numerical solutions of the problem follows the procedure shown in Sec. 3.1.3. Because ν_e is not known in advance, an iteration has to be conducted. Similar iteration has been designed in sec. 10 of Wang et al. (2015). Considering the platform length is comparable to water depth and wave length, a constant eddy viscosity coefficient ν_e , in terms of \mathcal{H} in (56) and (57), is used in present work. The values of \mathcal{H} are obtained from the numerical solution of the microscale cell problem discussed in Sec. 2.2.1.

The flow velocity under the platform induced by waves in the experimental scale is small as shown in Table 1 and so is the Keulegan-Carpenter number, defined by $K_C = \langle U' \rangle T' / d'$, where $\langle U' \rangle$ is the ambient velocity amplitude, T' the wave period and d' the cylinder diameter. We apply Eq.(42) to small K_C without using any fitting parameter because the influences of wave velocities at different oscillation phases, as well as the inertia effects, have been taken into accounted in $C_{D,rms}$. Bearman et al. (1985) gave the relation of force coefficient for circular cylinder with K_C number matching well with its inviscid value of $\sqrt{2}\pi^2/K_C$. It was found that the variation of force coefficient with small K_C was independent of $\beta = d^2/\nu T$, where β ranged from 196 to 1665. For our experimental tests, β varies from 1000 for $T = 0.9$ s and $Re = 672$, to 375 for $T = 2.4$ s and $Re = 1665$. Fig. 7 shows the variation of force coefficient vs Reynolds number $Re = \langle U' \rangle d' / \nu$ in our experiments. Within the range of Reynolds number in our laboratory experiments, the force coefficients lie between the lines predicted by $\sqrt{2}\pi^2/K_C$. There is significant difference between $C_{D,rms}$ and $C_{D\infty}$ when Reynolds number is small. For flows at large Reynolds number or K_C number, $C_{D,rms}$ gradually approaches $C_{D\infty}$.

Table 1

Parameters for 2D experiments. Wave amplitude $A' = 2$ cm, water depth $h' = 40$ cm, draft $D' = 10$ cm, platform length $2L' = 1.0$ m, cylinder diameter $a' = 3$ cm. $C_{D\infty}$ is calculated by the empirical formula (41). $K_C = \langle U' \rangle T' / a'$.

T' (s)	$k'h'$	$k'D'$	$k'L'$	$\langle U' \rangle$ (cm/s)	σ	$C_{D\infty}$	$C_{D,rms}$	Re_v	K_C
0.9	2.05	0.51	5.14	2.24	0.0027	1.55	10.84	4256	0.67
1.0	1.72	0.43	4.29	2.77	0.0035	1.46	8.48	5276	0.92
1.1	1.48	0.37	3.69	3.27	0.0039	1.41	6.96	6196	1.20
1.2	1.30	0.32	3.25	3.71	0.0040	1.37	5.89	7033	1.48
1.3	1.16	0.29	2.90	4.05	0.0048	1.35	5.23	7686	1.76
1.4	1.05	0.26	2.63	4.36	0.0051	1.33	4.72	8266	2.03
1.5	0.96	0.24	2.40	4.59	0.0053	1.32	4.36	8702	2.29
1.6	0.89	0.22	2.22	4.86	0.0054	1.31	4.05	9230	2.59
1.7	0.82	0.21	2.06	4.99	0.0059	1.30	3.82	9467	2.83
1.8	0.77	0.19	1.92	5.12	0.0064	1.30	3.63	9721	3.07
1.9	0.72	0.18	1.81	5.24	0.0066	1.29	3.47	9945	3.47
2.0	0.68	0.17	1.70	5.37	0.0069	1.29	3.33	10186	3.58
2.2	0.61	0.15	1.53	5.49	0.0074	1.29	3.12	10432	4.03
2.4	0.56	0.14	1.39	5.55	0.0079	1.29	2.96	10532	4.44



Fig. 6. Illustration of long platform supported by piles for 2D problem.

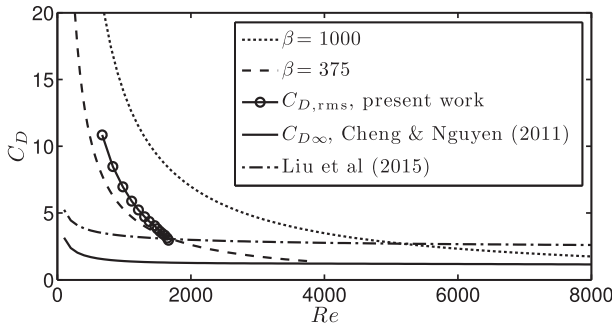


Fig. 7. The variation of force coefficient with Reynolds number $Re = \langle U' \rangle a' / \nu$. The dotted line and dashed line represent the relation of force coefficient and K_C number for $\beta = 1000$ and 375.

Fig. 8 compares the computed reflection and transmission coefficient with the experimental data. The reflection and transmission coefficients for a platform without piles are also displayed in the figure. It is obvious that the cylinder array dissipates much wave energy.

4. Scattering by a pile-group supported circular platform

The scattering problem around a circular platform without supporting piles has been well studied by Miles and Gilbert (1968); Garrett (1971); Miles (1971); Black et al. (1971) among others. The calculation of scattering problems around piles-supported platform can be viewed as an extension of the scattering problem around a platform in open water. We study the problem in the cylindrical coordinate system.

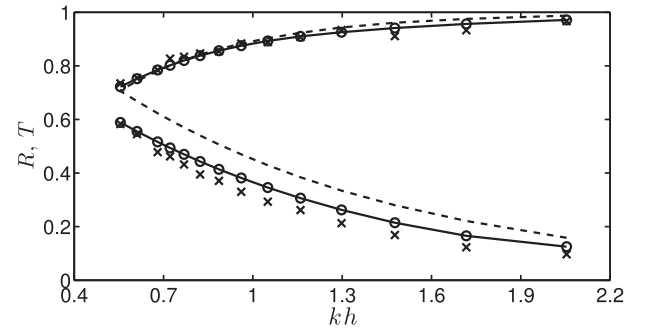


Fig. 8. Comparison between theoretical reflection and transmission coefficient and experimental data. $\ell' = 8$ cm, $a' = 3$ cm, $D' = 10$ cm, $h' = 40$ cm, $A' = 2$ cm. Solid line with circles represents the results predicted by present semi-analytical approach, cross is experimental results, dash line represents no cylinder condition based on the theory presented in Mei and Black (1969).

4.1. The inner region

The complete solution of pressure under platform is

$$\begin{aligned} \tilde{p}^{(0)}(r, \theta, Z) &= \sum_{n=0}^{\infty} P_n(r, \theta) F_n = \sum_{n=0}^{\infty} \sum_{m=0}^{\infty} R_{mn}(r) \cos m\theta F_n \\ &= \sum_{m=0}^{\infty} \mathcal{P}_m(r, Z) \cos m\theta \end{aligned} \quad (58)$$

with definition $P_n(r, \theta) = \sum_{m=0}^{\infty} R_{mn}(r) \cos m\theta$. We only need to consider the m -th component due to the orthogonal property of $\cos m\theta$. Substituting (58) into (32), we get

$$\frac{\partial^2 R_{mn}}{\partial r^2} + \frac{1}{r} \frac{\partial R_{mn}}{\partial r} - \frac{m^2}{r^2} R_{mn} - \frac{\mathcal{W}}{\mathcal{H}} K_n^2 R_{mn} = 0 \quad (59)$$

which is m -order modified Bessel equation with general solutions $I_m(\lambda_n r)$ and $K_m(\lambda_n r)$, and eigenvalues $\lambda_n = K_n \sqrt{\mathcal{W}/\mathcal{H}}$. Due to the finite value condition at $r = 0$ in the flow region, we have $R_{mn} = P_{mn} I_m(\lambda_n r) / I'_m(\lambda_n R)$ for convenience. If $n = 0$, the eigenvalue $K_0 = 0$, thus Eq. (59) reduces to Euler equation. At $r = 0$, the finite value condition of the general solution results in $R_{m0} = F_{m0}(r/R)^m$. Therefore, we have

$$\mathcal{P}_m(r, Z) = P_{m0} \left(\frac{r}{R} \right)^m F_0 + \sum_{n=1}^{\infty} P_{mn} \frac{I_m(\lambda_n r)}{I'_m(\lambda_n R)} F_n \quad (60)$$

4.1.1. Matching of velocity

At the interface between the cylinder array and the open water, we set $\langle u(R, z, \theta) \rangle = \sum_m \mathcal{U}_m(z) \cos m\theta$. According to $\mathcal{U}_m(Z) = -\mathcal{H} \partial \mathcal{P}_m / \partial r$ and (60), we obtain $\mathcal{U}_0(Z) = -\mathcal{H} \sum_n \lambda_n P_{0n} F_n$ and $\mathcal{U}_m(Z) = -\mathcal{H} (m P_{m0} F_0 + \sum_n \lambda_n P_{mn} F_n)$ for $m \geq 1$. Integrating $\mathcal{U}_m(Z)$ with F_n for $Z \in (-h, -D)$ and using the orthogonal property, we obtain

$$\langle \mathcal{U}_m, F_n \rangle = \begin{cases} -\mathcal{H} m P_{m0} & n = 0 \\ -\mathcal{H} \lambda_n P_{mn} & n \geq 1 \end{cases} \quad (61)$$

herein $m = 0, 1, 2, \dots$

On the open water side, the velocity $\mathcal{U}_m(Z)$ at $r = R$ can be calculated from $\mathcal{U}_m(Z) = \partial(\Phi_m^I + \Phi_m^R) / \partial r$ with potential functions Φ_m^I and Φ_m^R defined in (4) and (5). Integrating the product of $\mathcal{U}_m(Z)$ and f_n from $Z \in (-h, 0)$, we get

$$\langle \mathcal{U}_m, f_n \rangle = \begin{cases} -i^m \varepsilon_m k J'_m(kR) + Q_{m0} k & n = 0 \\ Q_{mn} k_n & n \geq 1 \end{cases} \quad (62)$$

4.1.2. Matching of potential

At $r = R$, we have $\mathcal{P}_m(R, z) = i[\Phi_m^I(R, z) + \Phi_m^R(R, z)]$ for $Z \in (-h, -D)$. For $m = 0$

$$\left[P_{00} F_0 + \sum_{n=1}^{\infty} P_{0n} \frac{I_0(\lambda_n R)}{I'_0(\lambda_n R)} F_n \right] = i \left[-f_0 J_0(kR) + Q_{00} \frac{H_0^{(1)}(kR)}{H_0^{(1)}(kR)} f_0 + \sum_{n=1}^{\infty} Q_{0n} \frac{K_0(k_n R)}{K'_0(k_n R)} f_n \right] \quad (63)$$

From relationship (62) and (61), we get

$$Q_{00} = \frac{\langle \mathcal{U}_0, f_0 \rangle}{k} + J'_0, \quad Q_{0n} = \frac{\langle \mathcal{U}_0, f_n \rangle}{k_n}, \quad P_{0n} = -\frac{\langle \mathcal{U}_0, F_n \rangle}{\mathcal{H} \lambda_n} \quad (64)$$

Note that P_{00} is the constant pressure beneath the platform and could not be explicit obtained from (61). By integrating (63) with $F_0(z)$ for $Z \in (-h, -D)$, we obtained:

$$P_{00} = i \left[\left(Q_{00} \frac{H_0^{(1)}(kR)}{H_0^{(1)}(kR)} - J_0(kR) \right) G_{00} + \sum_{n=1}^{\infty} Q_{0n} \frac{K_0(k_n R)}{K'_0(k_n R)} G_{n0} \right] \quad (65)$$

Physically, (65) implies that the constant pressure P_{00} beneath the platform is determined by the flow field of scattering problem determined from Φ_0^I and Φ_0^R , which are expressed in $J_0(kR)$ and Q_{0n} .

For $m = 1, 2, 3, \dots$

$$\begin{aligned} & \left[P_{m0} F_0 + \sum_{n=1}^{\infty} P_{mn} \frac{I_m(\lambda_n R)}{I'_m(\lambda_n R)} F_n \right] \\ &= i \left[-2f_0 i^m J_m(kR) + Q_{m0} \frac{H_m^{(1)}(kR)}{H_m^{(1)}(kR)} f_0 + \sum_{n=1}^{\infty} Q_{mn} \frac{K_m(k_n R)}{K'_m(k_n R)} f_n \right] \end{aligned} \quad (66)$$

From (61) and (62), we have

$$P_{m0} = -\frac{\langle \mathcal{U}_m, F_0 \rangle}{m \mathcal{H}}, \quad P_{mn} = -\frac{\langle \mathcal{U}_m, F_n \rangle}{\lambda_n \mathcal{H}} \quad (67)$$

$$Q_{m0} = \frac{\langle \mathcal{U}_m, f_0 \rangle}{k} + \varepsilon_m i^m J'_m(kR), \quad Q_{mn} = \frac{\langle \mathcal{U}_m, f_n \rangle}{k_n} \quad (68)$$

4.1.3. Solution procedure

We use Ritz method to solve the scattering problem. Define

$$\mathcal{U}_m(Z) = \sum_{s=0}^S A_{ms} F_s(Z) \quad (S \leq N) \quad (69)$$

At position $Z_s \in (-h, -D)$, we have following conditions:

For $m = 0$, Eq.(63) reads

$$\begin{aligned} & -\sum_{n=1}^S \frac{A_{0n}}{\lambda_n \mathcal{H}} \frac{I_0}{I'_0} F_n(Z_s) \\ &= i \left[\left(\frac{H_0^{(1)}}{H_0^{(1)}} \left(\frac{\sum_{s=0}^S A_{0s} G_{0s}}{k} + J'_0 \right) - J_0 \right) (f_0(Z_s) - G_{00} F_0(Z_s)) \right. \\ & \quad \left. + \sum_{n=1}^N \frac{\sum_{s=0}^S A_{0s} G_{ns}}{k_n} \frac{K_0}{K'_0} (f_n(Z_s) - G_{n0} F_0(Z_s)) \right] \end{aligned} \quad (70)$$

and for $m \geq 1$ Eq.(66) reads

$$\begin{aligned} & -\frac{A_{m0}}{m \mathcal{H}} F_0(Z_s) - \sum_{n=1}^S \frac{A_{mn}}{\lambda_n \mathcal{H}} \frac{I_m}{I'_m} F_n(Z_s) \\ &= i \left[\left(\frac{H_m^{(1)}}{H_m^{(1)}} \left(\frac{\sum_{s=0}^S A_{ms} G_{0s}}{k} + 2i^m J'_m \right) - 2i^m J_m \right) f_0(Z_s) \right. \\ & \quad \left. + \sum_{n=1}^N \frac{\sum_{s=0}^S A_{ms} G_{ns}}{k_n} \frac{K_m}{K'_m} f_n(Z_s) \right] \end{aligned} \quad (71)$$

with $G_{ns} = \langle f_n, F_s \rangle$. Solving the linear equations set of dimension $S + 1$ composed of (70) and (71), we can obtained the coefficient A_{ms} for $s = 0, 1, \dots, S$.

After obtaining the value of A_{ms} , the coefficient of scattering wave potential can be evaluated from the definition (64), (68) and (69) by $Q_{m0} = \sum_{s=0}^S A_{ms} G_{0s} / k + i^m \varepsilon_m J'_m$ and $Q_{mn} = \sum_{s=0}^S A_{ms} G_{ns} / k_n$ for $m \geq 0$. Due to the orthogonal property of eigenfunction F_n , P_{mn} ($m = 0, 1, \dots$; $n = 1, 2, \dots$) can be calculated from (67) as $P_{mn} = -A_{mn} / \lambda_n \mathcal{H}$ for $1 \leq n \leq S$ and $P_{mn} = 0$ for $n > S$. Value of P_{m0} ($m = 1, 2, \dots$) can be calculated from (67) as $P_{m0} = -A_{m0} / m \mathcal{H}$, and P_{00} can be obtained from (65). Now we have obtained the pressure distribution for calculating the hydrodynamics loads.

4.2. Calculations of the hydrodynamic loads

In dimensional form, the pressure in clear water region can be calculated from the total potential $p(r, \theta, z) = i\omega \rho \phi$. For clear water under a platform, the constant term is related to that part of the pressure under the platform which is independent of position and contributes nearly all the vertical force on the platform. By defining $B = \pi R^2 \rho g \mathcal{A}$ (the hydrostatic buoyancy force associated with a free surface wave amplitude \mathcal{A} over the platform), the total dimensionless vertical force is

$$\frac{\mathcal{F}_z}{B} = \frac{1}{\pi R^2} \int_0^R \mathcal{P}_0(r, -D) 2\pi r dr \quad (72)$$

The dimensionless horizontal force at x-direction ($r \cos \theta$) can be calculated by surface integrating the pressure P_w for $Z \in (-D, 0)$ at $r = R$ by

$$\frac{\mathcal{F}_x}{B} = \frac{1}{\pi R^2} \int_0^{2\pi} \int_{-D}^0 P_w \cos \theta R d\theta dZ \quad (73)$$

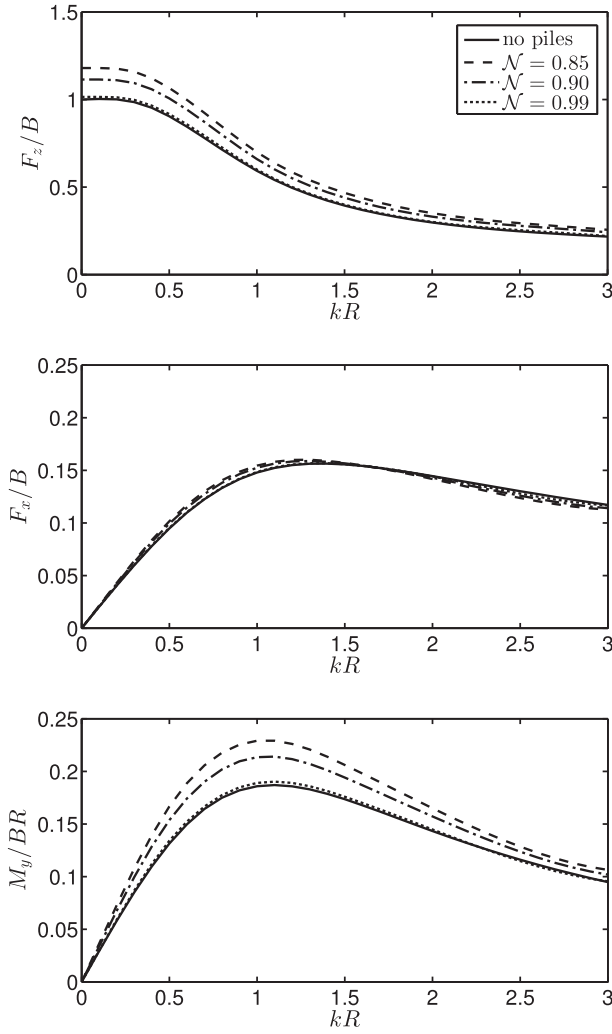


Fig. 9. Comparisons of hydrodynamic forces and transversal torque on the platform for different porosity. Parameters are $h = 1$, $R = 1$, $D = 1/6$. The force calculation for no pile case is based on the theory presented in Mei and Black (1969).

Table 2

Input parameters of selected cases, $a' = 1$ m, $N = 0.85$, wave amplitude $A' = 4$ m, water depth $h' = 30$ m, draft $D' = 5$ m, and the radius of the circular platform $R' = 30$ m.

T' (s)	kh	λ' (m)	$\langle U' \rangle$ (m/s)	Re	Re_v	$C_{D,rms}$	K_C	σ
37	0.3	628	0.23	2.3e5	1.0e6	1.43	8.55	0.0008
23	0.5	377	0.59	5.9e5	2.7e6	1.15	13.5	0.0016
13	1.0	189	1.70	1.7e6	7.7e6	0.96	21.4	0.0028
9.4	1.5	127	2.5	2.5e6	1.1e7	0.93	23.6	0.0042
7.9	2.0	94	2.8	2.8e6	1.3e7	0.94	22.0	0.0074
6.4	3.0	63	2.65	2.6e6	1.2e7	1.00	16.9	0.0160

with $P_w = i(\Phi_1^I + \Phi_1^R)\cos\theta$. Here only potential functions relating $\cos\theta$ are retained due to the orthogonal property of cosine functions in $\theta \in (0, 2\pi)$.

The transversal torque in y-direction respect to the bottom center is contributed from two parts: one part is due to the pressure at the bottom of the platform, $M_y^{(b)}$ calculated as:

$$\mathcal{A} \frac{M_y^{(b)}}{BR} = \frac{1}{\pi R^3} \int_0^{2\pi} \int_0^R \mathcal{P}_1(r, -D) \cos^2 \theta r^2 dr d\theta \quad (74)$$

Another part is due to the pressure force at the side of the platform $M_y^{(s)}$

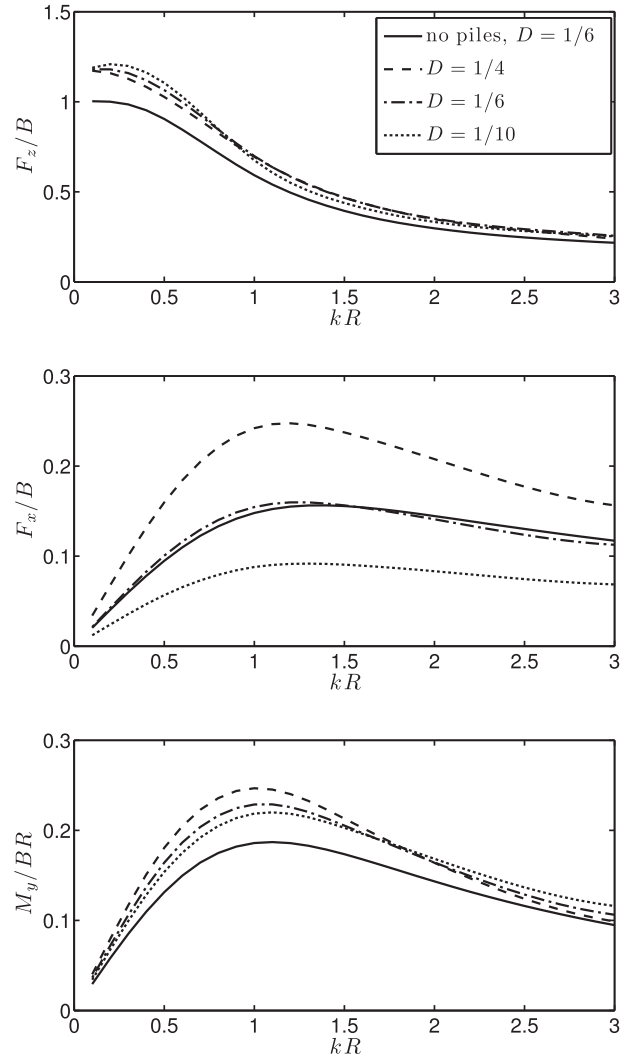


Fig. 10. Comparisons of hydrodynamic forces and transversal torque on the platform for different draft, $h = 1$, $R = 1$, $N = 0.85$. The force calculation for no pile case is based on the theory presented in Mei and Black (1969).

$$\mathcal{A} \frac{M_y^{(s)}}{BR} = \frac{1}{\pi R^3} \int_0^{2\pi} \int_{-D}^0 P_w \cos \theta R(Z + D) d\theta dZ \quad (75)$$

4.3. Numerical results of hydrodynamic loads

The series expansion (58) representing the pressure under the platform was truncated after N and S terms. It was found that $N = 200$ and $S = 200$ ensured convergence with a relative error less than $1.0E-4$.

The force on the pile-group supported platform in the circumstances of wave flow is of course different from those without piles. Here we investigate the influence of piles porosity and draft on vertical, horizontal force and transversal torque. Fig. 9 shows the vertical force, the horizontal force and the transversal torque exerted on the platform as functions of kR for different pile-group porosity under the same draft. The main input parameters for selected cases are listed in Table 2. In the figure, the forces and transversal torque imposed on the circular platform without supported piles are presented as well for references.

The pile porosity has obvious effect on the vertical force and transversal torque, while the influence on horizontal force is negligible. As expected, the influence gradually fades when the porosity tends to 1. For the vertical force, the maximum amplitude is larger for a denser pile group, i.e. a lower porosity N , which occurs at $kR \rightarrow 0$. When porosity $N = 1$, the maximum amplitude tends to the hydrostatic buoyancy force.

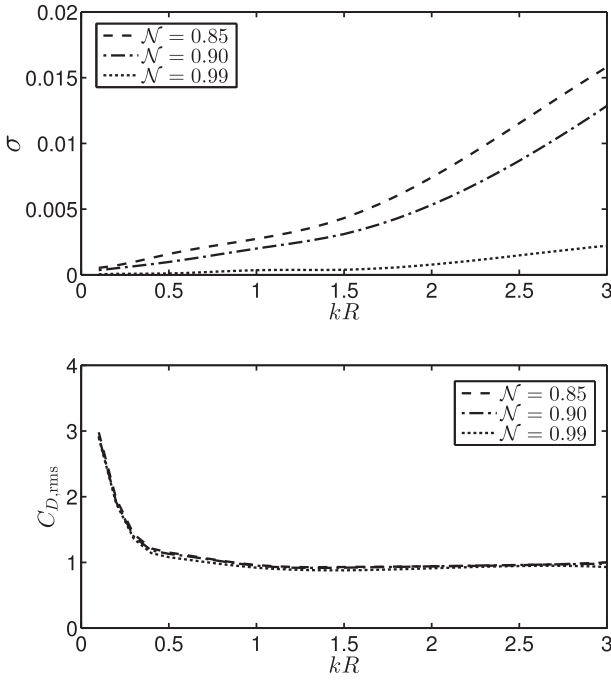


Fig. 11. The viscosity parameter and the drag coefficient on pile groups of different porosity \mathcal{N} and wave number k , for $h = 1$, $R = 1$, $D = 1/6$.

The maximum increase of vertical force can reach up to 18% for $\mathcal{N} = 0.85$. Denser pile group may result in even larger vertical force.

The transversal torque on the platform behaves in a similar way as the horizontal force, reaching its maximum amplitude when kR close to 1. The values of transversal torque are more sensitive to the porosity, in the same manner as that of vertical force.

Fig. 10 shows the vertical force, horizontal force and transversal torque against wave parameter kR with varying draft. Setting the result with draft $D = 1/6$ for open water flow as a reference, it is apparent that changing the draft does not noticeably affect the vertical force and transversal torque, but has much influence on the horizontal force. It is understandable that the horizontal force is roughly proportional to the draft of the platform D , because of the linear relationship between the drag force F_x and the projected area $2RD$. The important conclusion from Figs. 9 and 10 is that vertical force and transversal torque are more influenced by the viscous effect due to the presence of the pile group.

Numerical results for σ and $C_{D,rms}$ are shown in Fig. 11. The averaged dimensionless viscosity σ decreases with the porosity \mathcal{N} . For the same porosity, the viscous effect is weak for $kR \leq 1$ and then increases rapidly for large kR signifying the stronger turbulence flow within the pile group. While the averaged drag coefficient $C_{D,rms}$ almost remains constant close

to 1 except for very long wave $kR \rightarrow 0$, which is nearly independent of porosity \mathcal{N} for the sparse pile array.

Depending on the direction of the incident waves, the flow patterns can vary between in-line arrays and staggered arrays. The mean drag coefficient should be different. The values of \mathcal{K} and \mathcal{W} depend on the angle between the incident wave and cylinder arrays as discussed in Guo et al. (2014). Cases other than in-line arrays can be computed by modifying the cell problem accordingly.

5. Conclusions

In the present paper, the homogenization method initiated in Mei et al. (2014) and Liu et al. (2015) is extended to investigate wave scattering around a pile-group supported platform. The macro scale wave dynamics under the platform is solved from the cell-averaged pressure Eq. (32) in the form of homogeneous and anisotropic Laplace equation, which contains coefficients that are computed from micro-scale flows for a unit cell. The boundary-value-problem for micro-scale flows is derived from the linearized Reynolds equations with constant eddy viscosity model, which provides the dissipation mechanism due to turbulence and saves much more computational efforts than direct numerical simulations.

To determine the constant bulk eddy viscosity in the calculations, the root mean square force coefficient including the influences of oscillating velocities at different phase and inertia effect is adopted by using the experimental data of Bearman et al. (1979) for plane oscillating flow. Validations of the present model are confirmed by existing theories of platform without supported piles, and by our 2D experiments for pile-group supported platform. Good agreements of these comparisons demonstrate the effectiveness of the proposed method.

Finally, field-scale wave scattering by a pile-group supported circular platform is examined for different porosity, draft and wave parameters. Numerical results indicate that the pile porosity has remarkable effects on the vertical force and the transversal torque, and the influence increases with decreasing porosity. The maximum vertical force occurs at $kR \rightarrow 0$, while the maximum horizontal force is obtained at kR close to 1. Draft of the platform shows significant influence on horizontal force proportional to the projected area in wave direction, but negligible effect on vertical force and transversal torque. It is apparent that the vertical force and transversal torque are influenced by the pressure distribution inside the pile group and viscous effect due to the existence of pile group.

Acknowledgements

This work was jointly supported by the Key Doctoral Program Foundation of Shanghai Municipality (No. B206), the National Program on Key Basic Research Project (973 Program No. 2013CB036102) and the Chinese National Science Foundation (Grant No. 11572193).

Appendix A. Evaluation of α_{ik} and β

For the evaluation of α_{ik} and β , we use the following procedure instead of calculating them from the definition.

Taking α_{21} as an example, let us calculate from:

$$\alpha_{21} = -\oint ds A_1 n_2 + 2\sigma \oint ds \frac{\partial K_{21}}{\partial x_2} n_2 + \sigma \oint ds \frac{\partial K_{21}}{\partial x_1} n_1 + \sigma \oint ds \frac{\partial K_{11}}{\partial x_2} n_1 \quad (\text{A.1})$$

- $\oint ds A_1 n_2$: From Fig. A.12, we can see that A_1 is symmetry versus $y=0$ and n_2 is the y component of outward normal vector along the cylinder surface. Thus the integrals in the upper half plane and the lower half plane are canceled.
- $\oint ds \frac{\partial K_{21}}{\partial x_2} n_2$ and $\oint ds \frac{\partial K_{21}}{\partial x_1} n_1$: K_{21} is antisymmetrical about both axes. $\partial K_{21} / \partial x_2$ is symmetric versus $y=0$, so the integrations in the upper half plane and lower half plane are balanced. $\partial K_{21} / \partial x_1$ is symmetric about $x=0$, so the integrations in the right half plane and left half plane in each side of $x = 0$ are balanced. Numerical computation verifies the symmetry properties and integration value.

- $\oint ds \frac{\partial K_{11}}{\partial x_2} n_1$: From Fig. A.12, K_{11} are symmetrical about $y = 0$, hence values of $\frac{\partial K_{11}}{\partial x_2}$ take opposite sign in the upper half plane and lower half plane. They are canceled in each side of $x = 0$.

From the computed value shown in Fig. A.12, we observed that the flow fields caused by the macro scale pressure gradients $\partial \bar{p}^{(0)} / \partial X_1$ and $\partial \bar{p}^{(0)} / \partial X_2$ have exactly the same distribution except for a 90° rotation. The value of α_{12} can be calculated in a similar procedures as that of α_{21} . Therefore we have another important properties of α_{ik} .

$$\alpha_{12} = \alpha_{21} = 0 \quad (\text{A.2})$$

These properties hold for other array geometries symmetrical about both axes.

The cell problem on the microscale is similar to Stokes flow of small Reynolds numbers. The line integration in (29) is the summation of viscous force and normal pressure force along the cylinder surface. We know there is no lift force on a circular cylinder for Stokes flow. Therefore $\alpha_{ik} = 0$ when $i \neq k$. This conclusion is only valid when there is geometry in both x, y directions. Otherwise the lift force can not cancelled. The value of α_{11} and α_{22} represent the corresponding drag forces, which can be interpreted as the drag coefficient.

Next we prove that α_{11} and α_{22} are identical. If we substitute relationship (18) into cell averaged horizontal momentum Eq. (27), and with $\alpha_{12} = 0$, $\langle K_{12} \rangle = 0$ and $\langle K_{21} \rangle = 0$, we have

$$\alpha_{11} = -\mathcal{N} - i\langle K_{11} \rangle \quad (\text{A.3})$$

In a similar approach, we have

$$\alpha_{22} = -\mathcal{N} - i\langle K_{22} \rangle \quad (\text{A.4})$$

Physically, the distribution of K_{11} and K_{22} are same except there is a $\pi/2$ rotation in physical space. Consequently, we have $\alpha_{11} = \alpha_{22} = -\mathcal{N} - i\mathcal{W}$. If we substitute relationship (18) into cell averaged vertical momentum Eq. (28), we get

$$\beta = -\mathcal{N} - i\langle W \rangle = -\mathcal{N} - i\mathcal{W} \quad (\text{A.5})$$

Directly computing α_{ik} and β from their definition Eqs. (29) and (30) gives identical results using Eqs. (A.3)–(A.5).

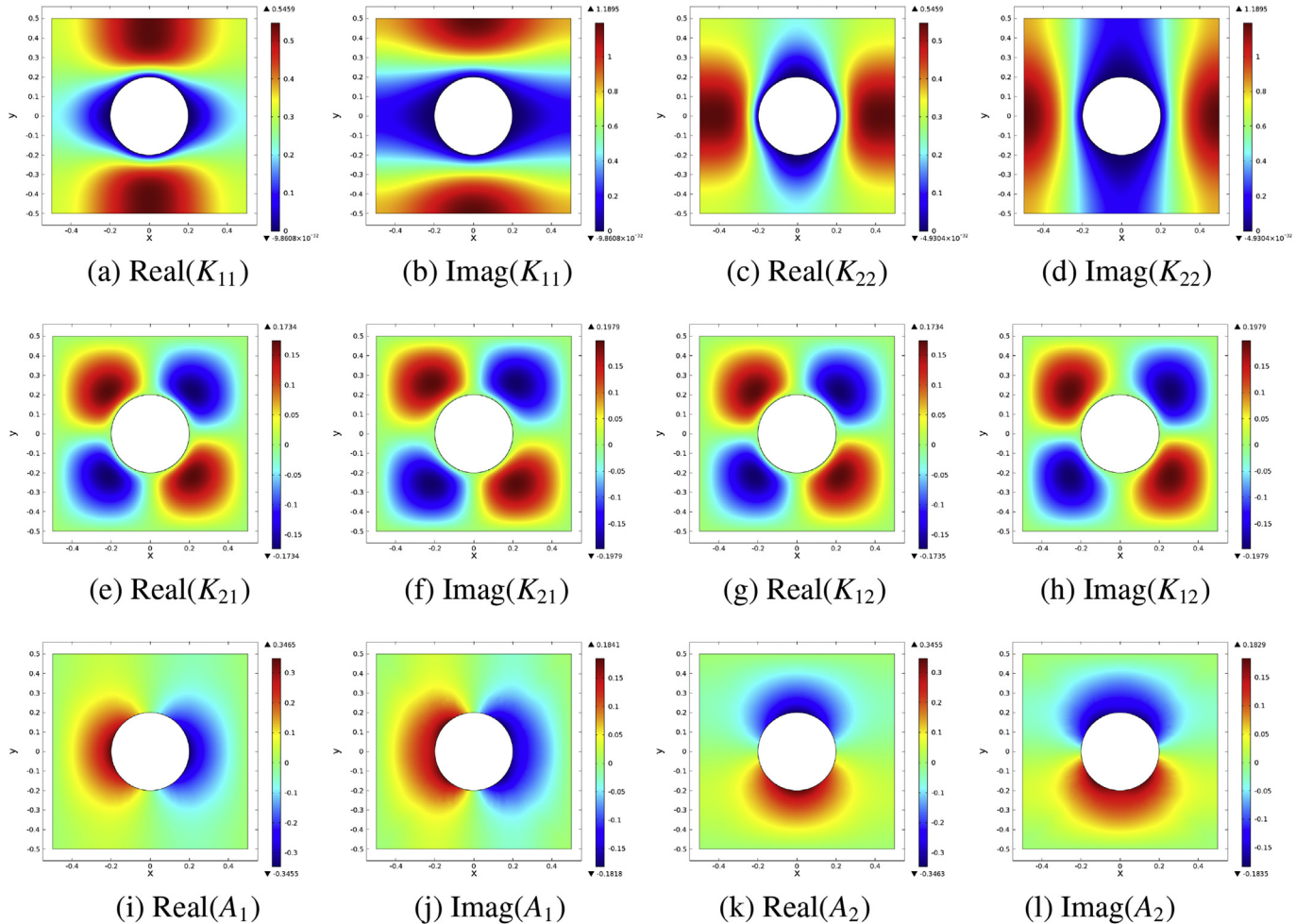


Fig. A.12. Illustration of FEM solutions for K_{ij} and A_j . From numerical results, $\langle K_{11} \rangle = \langle K_{22} \rangle = 0.3134 + 0.5764i$, $\langle K_{12} \rangle = \langle K_{21} \rangle = 0$. For A_j , we compare the gradient value, and obtain $\langle \partial A_1 / \partial x \rangle = \langle \partial A_2 / \partial y \rangle = 0.2506 + 0.1416i$. Parameters are: cylinder radius $r = 0.2$, porosity $n = 0.8743$, and dimensionless viscous coefficient $\sigma = 0.0259$.

References

- Bearman, P.W., Graham, J.M.R., Sing, S., 1979. Forces on cylinders in harmonically oscillating flow. In: Shaw, T.L. (Ed.), *Proc. Mechanics of Wave-induced Forces on Cylinders*. Pitman, London, pp. 437–449.
- Bearman, P.W., Downie, M.J., Graham, J.M.R., Obasaju, E.D., 1985. Forces on cylinders in viscous oscillatory flow at low Keulegan-Carpenter numbers. *J. Fluid Mech.* 154, 337–356.
- Black, J.L., Mei, C.C., Bray, M.C.G., 1971. Radiation and scattering of water waves by rigid bodies. *J. Fluid Mech.* 46 (1), 151–164.
- Bonakdar, L., Oumeraci, H., 2012. Interaction of waves and pile group-supported offshore structures: a large scale model study. In: *Proceedings of the Twenty-second International Offshore and Polar Engineering Conference*, 2012, Rhodes, Greece, pp. 812–818.
- Bonakdar, L., Oumeraci, H., 2015. Pile group effect on the wave loading of a slender pile: a small-scale model study. *Ocean. Eng.* 108, 449–461.
- Chen, J.T., Lee, J.W., 2013. A near-trapped mode and fictitious frequencies of multiple scattering by an array of elliptical cylinders in water waves. *Phys. Fluids* 25 (9), 079103.
- Chen, J.T., Lin, Y.J., Lee, Y.T., Wu, C.F., 2011. Water wave interaction with surface-piercing porous cylinders using null-field integral equations. *Ocean. Eng.* 38, 409–418.
- Cheng, N.S., Nguyen, H.T., 2011. Hydraulic radius for evaluating resistance induced by simulated emergent vegetation in open-channel flows. *J. Hydraul. Eng.* 137 (9), 995–1004.
- Faltinsen, O.M., 1998. *Sea Loads on Ships and Offshore Structures*. Cambridge University Press, pp. 245–249.
- Garrett, C., 1971. Wave forces on a circular dock. *J. Fluid Mech.* 46 (1), 129–139.
- Goda, Y., Suzuki, Y., 1976. Estimation of incident and reflected waves in random wave experiments. In: *Proc. 15th Coastal Engrg. Conf.*, 1, pp. 828–845.
- Guo, X.Y., Wang, B.L., Mei, C.C., 2014. Flow and solute transport through a periodic array of vertical cylinders in shallow water. *J. Fluid Mech.* 756, 903–934.
- Kagemoto, H., Yue, D.K.P., 1986. Interactions among multiple three-dimensional bodies in water waves: an exact algebraic method. *J. Fluid Mech.* 166, 189–209.
- Kagemoto, H., Yue, D.K.P., 1993. Hydrodynamic interaction analysis of very large floating structures. *Mar. Struct.* 6 (2-3), 295–322.
- Kashiwagi, M., 2000. Hydrodynamic interactions among a great number of columns supporting a very large flexible structure. *J. Fluids Struct.* 14, 1013–1034.
- Lamas-Pardo, M., Iglesias, G., Carral, L., 2015. A review of very large floating structures (VLFS) for coastal and offshore uses. *Ocean. Eng.* 109, 677–690.
- Lintion, C.M., 2001. The finite dock problem. *Z. Angew. Math. Phys.* 52, 640–656.
- Lintion, C.M., Evans, D.V., 1990. The interaction of waves with arrays of vertical circular cylinders. *J. Fluid Mech.* 215, 549–569.
- Liu, P.L.-F., Chang, C.W., Mei, C.C., Lomonaco, P., Martin, F.L., Maza, M., 2015. Periodic water waves through an aquatic forest. *Coast. Eng.* 96, 100–117.
- Maull, D.J., Milliner, M.G., 1978. Sinusoidal flow past a circular cylinder. *Coast. Eng.* 2, 149–168.
- Mei, C.C., Black, J.L., 1969. Scattering of surface waves by rectangular obstacles in waters of finite depth. *J. Fluid Mech.* 38 (3), 499–511.
- Mei, C.C., Stiassnie, M., Yue, D.K.P., 2005. *Theory and Applications of Ocean Surface Waves. Part 1: Linear Aspects*, p. 362.
- Mei, C.C., Chan, I.-C., Liu, P.L.-F., Huang, Z., Zhang, W., 2011. Long waves through emergent coastal vegetation. *J. Fluid Mech.* 687, 461–491.
- Mei, C.C., Chan, I.-C., Liu, P.L.-F., 2014. Waves of intermediate length through an array of vertical cylinders. *Environ. Fluid Mech.* 14, 235–261.
- Miles, J.W., 1971. A note on variational principles for surface-wave scattering. *J. Fluid Mech.* 46, 141–149.
- Miles, J.W., Gilbert, J.F., 1968. Scattering of gravity waves by a circular dock. *J. Fluid Mech.* 34, 783–793.
- Porter, R., 2016. Surface wave interaction with rigid plates lying on water. *Wave Motion* 66, 118–131.
- Simon, M.J., 1982. Multiple scattering in arrays of axisymmetric wave-energy devices. Part 1. A matrix method using a plane-wave approximation. *J. Fluid Mech.* 120, 1–25.
- Singh, J., Babarit, A., 2014. A fast approach coupling boundary element method and plane wave approximation for wave interaction analysis in sparse arrays of wave energy converters. *Ocean. Eng.* 85, 12–20.
- Spring, B.H., Monkmeyer, P.L., 1974. Interaction of plane waves with vertical cylinders. In: *Proceedings 14th International Coastal Engineering Conference*, Copenhagen, Denmark, pp. 1828–1847.
- Stoker, J.J., 1958. *Water Waves: the Mathematical Theory with Applications*. John Wiley & Sons, Inc.
- Wang, C.M., Tay, Z.Y., 2011. Very large floating structures, applications, research and development. *Proced. Eng.* 14, 62–72.
- Wang, B.L., Guo, X.Y., Mei, C.C., 2015. Surface water waves over a shallow canopy. *J. Fluid Mech.* 768, 572–599.
- Watanabe, W., Utsunomiya, T., Wang, C.M., 2004. Hydroelastic analysis of pooton-type VLFS: a literature survey. *Eng. Struct.* 26, 245–256.